

Impedance-Model-Based SSR Analysis for Type 3 Wind Generator and Series-Compensated Network

Zhixin Miao, *Senior Member, IEEE*

Abstract—Interaction between doubly fed induction generator (DFIG) Type 3 wind generators and series-compensated networks can lead to subsynchronous resonance (SSR) oscillations—a phenomenon observed in the real world. In this paper, impedance-based Nyquist stability criterion is applied to analyze the SSR phenomena. Impedance models of a DFIG along with its rotor-side converter (RSC) and grid-side converter, and a series-compensated network are derived in terms of space vectors. The DFIG impedance and the network impedance are analyzed to show the impact of wind speed, compensation level, and RSC current controller gain on SSR stability. Nyquist maps are also used to demonstrate the impact on SSR stability. Simulation studies are carried out to show SSR controller interaction. This paper successfully demonstrates that the interaction between the electric network and the converter controller is a leading cause of the SSR phenomena recently observed in wind generation grid integration.

Index Terms—Doubly fed induction generator (DFIG), impedance model, Nyquist criterion, subsynchronous resonance (SSR), wind generation.

I. INTRODUCTION

SUBSYNCHRONOUS resonance (SSR) oscillations have been observed in wind farms by the industry recently [1]–[3]. The incidents can cause damage to equipment and wind farms. Hence, SSR stability evaluation has been conducted in several industry reports [4], [5]. The study conducted by ABB for ERCOT CREZ system indicates that Type 3 or doubly fed induction generator (DFIG) wind generators are especially vulnerable to SSR instability [4]. In [3], an event that led to such phenomena was described and the recorded voltage and current waveforms with SSR oscillations are presented. A Type 3 wind farm is connected to a transmission path with two parallel lines. One line is equipped with series compensation (fixed capacitors). Due to a fault, the other line was tripped and the compensated line is radially connected to the wind farm. SSR oscillations started and aggravated.

Studies on SSR indicated that the phenomena are due to the interaction among the Type 3 induction generator and (or) power electronic converter control and the series-compensated line [3], [6], [7]. The interaction between the converter control and the series-compensated line is called subsynchronous control interaction (SSCI) in the literature. The SSR phenomena

in Type 3 wind farms are considered to be not related to wind turbine torsional interaction and are mainly electrical system phenomena.

Unlike the industry studies focusing on PSCAD-based time-domain simulation, in [8] and [9], nonlinear models in differential algebraic equation are built for a Type 3 wind farm radially connected to a series-compensated line. The DFIG is modeled in DQ reference frame. The converters are modeled using an average model and the controls are also modeled. The nonlinear system is linearized at various operating conditions. Eigenvalue analysis is then applied for stability check. Major findings from [9] are summarized as follows.

- 1) Torsional interactions between the network mode and the wind turbine torsional mode are rare. This is because the wind turbine has a soft shaft and the frequency of the torsional mode is quite low (< 3 Hz). In order to have torsional interactions, the network has to have a very high compensation level to reach a high network frequency (> 47 Hz).
- 2) Induction generator effect (IGE) is the major cause of SSR. This could be due to a negative slip at the SSR frequency which leads to a negative equivalent rotor resistance at low wind speeds. The negative feedback current controls also have adverse impact on stability.

Similar model-based simulation and eigenvalue-based analysis for a Type 3 wind generator with radial connected compensated line can be found in [10] and [11].

In [3] and [9], the authors addressed two possible SSR scenarios: low and high wind speed scenarios. In both scenarios, SSR instability can happen due to electrical system interactions whether it is IGE or SSCI.

To investigate electric system interactions including IGE and SSCI, impedance-based models, and Nyquist stability criterion provide insights. Such methods have been widely adopted in power electronics and system interaction studies [12], [13]. More recently, interactions between GSC current controllers and large network inductance have been addressed in [14] using impedance models.

The objective of this paper is to apply Nyquist stability criterion in analyzing Type 3 wind generator SSR phenomena. The analysis of this paper is centered on electrical system resonances including IGE and SSCI. Electric system resonances can be successfully studied using impedance-model-based analysis. Hence, impedance models will be developed for stability analysis. The preliminary work has been presented in [15], where a simplified impedance model for a DFIG was developed based on the per-phase induction machine circuit model. The slip is expressed in Laplace domain by intuition. Rotor-side

Manuscript received March 10, 2012; revised July 12, 2012; accepted July 23, 2012. Date of publication August 23, 2012; date of current version November 16, 2012. Paper no. TEC-00102-2012.

The author is with the Department of Electrical Engineering, University of South Florida, Tampa, FL 33620 USA (e-mail: zmiao@usf.edu).

Color versions of one or more of the figures in this paper are available online at <http://ieeexplore.ieee.org>.

Digital Object Identifier 10.1109/TEC.2012.2211019

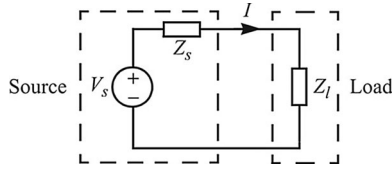


Fig. 1. Small-signal representation of a voltage source and a load [13].

converter (RSC) and grid-side converter (GSC) models are ignored. Nyquist stability criterion is applied to demonstrate SSR stability at different wind speeds.

In this paper, detailed impedance models of a DFIG along with its RSC and GSC current controllers will be developed. Since the converters' outer power/voltage loop has a much slower bandwidth compared to the SSR dynamics and the inner current control loop bandwidth, these controls are ignored in the impedance models. The popularly used *DQ0*-based induction machine model will be used as the starting point. While the series-compensated network can be considered as an *RLC* network with an impedance model $(R + sL + \frac{1}{sC})$, the two systems (the network and the DFIG) are not modeled in the same reference frame. To be able to apply Nyquist criterion, both impedance models will be transferred to the space vector platform. Impedance model developing is the foremost contribution of the paper.

With the developed models, impacts of wind speed, compensation level, and current controller gain on SSR stability will be carried out. The analysis of the paper can explain both low and high wind speed SSR phenomena. The rest of the paper is organized as follows. Section II introduces the concept of impedance-based Nyquist stability criterion. Section III presents the impedance models. Section IV presents SSR stability analysis applying Nyquist stability criterion and examines the impact of wind speed, compensation degree and RSC PI controller gain. Section V presents the simulation results and Section VI concludes this paper.

II. IMPEDANCE-BASED NYQUIST STABILITY CRITERION

Impedance-based small-signal analysis has been applied in power electronic converter analysis in [12] and [13]. For a system with a source impedance and load impedance, as shown in Fig. 1, the current can be found:

$$I(s) = \frac{V(s)}{Z_s(s) + Z_l(s)} \quad (1)$$

$$= \frac{V(s)}{Z_l(s)} \cdot \frac{1}{1 + Z_s(s)/Z_l(s)}. \quad (2)$$

Assume that the voltage source is stable and the load is stable when powered from an ideal voltage source; then for the system to be stable, the denominator $1 + Z_s(s)/Z_l(s)$ should have all zeros in the open left-half-plane. Based on Nyquist stability criterion, if and only if the number of counterclockwise encirclement around $(-1, 0)$ of Z_s/Z_l is equal to the number of the right-half-plane (RHP) poles of Z_s/Z_l , the system will be

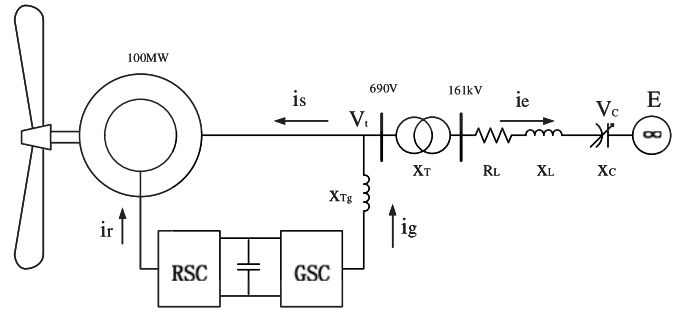


Fig. 2. Study system. The rated power of the wind farm is 100 MVA. The nominal voltage of the wind farm terminal bus is 690 V and the nominal voltage of the network is 161 kV.

stable. In cases when Z_s/Z_l has no RHP poles, the Nyquist map of Z_s/Z_l should not encircle $(-1, 0)$.

Instability happens when Z_s/Z_l encircles $(-1, 0)$. In addition, Bode plots can be used to analyze resonance stability. Bode plots of the source impedance and the load impedance can be placed together to identify the phase margin when the magnitudes of the two impedances are the same.

III. IMPEDANCE MODELS

A study system consisting of a Type 3 DFIG-based wind generator with partial back-to-back voltage source converters and series-compensated network has been studied in [9] and is shown in Fig. 2. A DFIG-based wind farm (100 MW from aggregation of 2-MW units) is connected to a 161-kV series-compensated line. The collective behavior of a group of wind turbines is represented by an equivalent lumped machine. X_{tg} represents the inductive filter at the GSC.

The impedance models for the series-compensated network and the DFIG system will be developed in this section. For a three-phase system, impedance model can be expressed in either space vector or *DQ0* synchronous reference frame. A space vector voltage relates to the instantaneous three-phase voltages as follows:

$$\vec{V} = v_a + \alpha v_b + \alpha^2 v_c \quad (3)$$

where $\alpha = e^{j\frac{2\pi}{3}}$.

A. RLC Circuit Impedance Model

Assume that the series-compensated network has no mutual inductance and the three phases are symmetrical. For such a three-phase *RLC* circuit, the impedance model observed in space vector can be expressed as

$$Z_{\text{net}} = \frac{\vec{V}}{\vec{I}} = \frac{v_a}{i_a} \quad (4)$$

$$= R + sL + \frac{1}{sC}. \quad (5)$$

B. Induction Machine Impedance Model

This section is devoted to develop the impedance model of an induction machine based on the widely known *DQ0* model

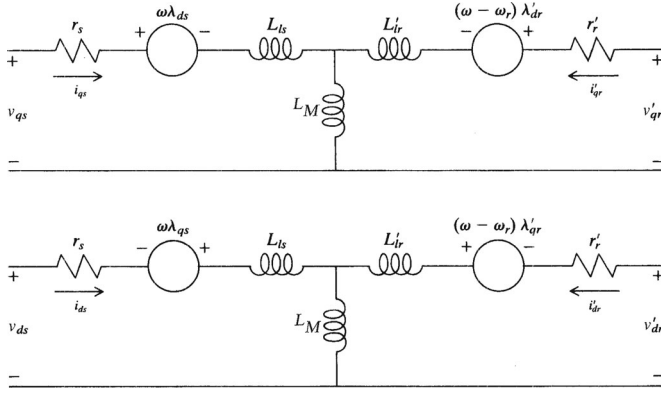


Fig. 3. qd -axis induction machine circuits [16].

presented in the classic textbook [16]. The qd -axis circuits are shown in Fig. 3.

The stator voltage, current, and flux linkage relation can be expressed as

$$\begin{aligned} v_{qs} &= r_s i_{qs} + \omega \lambda_{ds} + p \lambda_{qs} \\ v_{ds} &= r_s i_{ds} - \omega \lambda_{qs} + p \lambda_{ds} \end{aligned} \quad (6)$$

where p is the differential operator d/dt

$$\begin{aligned} \lambda_{qs} &= L_{ls} i_{qs} + L_M (i_{qs} + i'_{qr}) \\ \lambda_{ds} &= L_{ls} i_{ds} + L_M (i_{ds} + i'_{dr}). \end{aligned} \quad (7)$$

The rotor voltage, current, and flux linkage relation can be expressed as

$$\begin{aligned} v'_{qr} &= r'_r i_{qr} + (\omega - \omega_m) \lambda'_{dr} + p \lambda_{qr} \\ v'_{dr} &= r'_r i_{dr} - (\omega - \omega_m) \lambda'_{qr} + p \lambda_{dr} \end{aligned} \quad (8)$$

where ω is the nominal angular speed (377 rad/s), ω_m is the rotor angular speed, and

$$\begin{aligned} \lambda'_{qr} &= L'_{lr} i'_{qr} + L_M (i_{qs} + i'_{qr}) \\ \lambda'_{dr} &= L'_{lr} i'_{dr} + L_M (i_{ds} + i'_{dr}). \end{aligned} \quad (9)$$

The rotor currents in (6) can be substituted by expressions in terms of the stator currents and the rotor voltage. Two complex vectors $\vec{V}_{qds} = v_q - jv_d$ and $\vec{I}_{qds} = i_q - ji_d$ are defined. They are related to the space vector \vec{V} through the following relationship:

$$\vec{V} = \vec{V}_{qds} e^{j\omega t} \quad (10)$$

where $\vec{V} = v_a + \alpha v_b + \alpha^2 v_c$ and $\alpha = e^{j\frac{2\pi}{3}}$. For a positive sequence, the corresponding space vector is a counterclockwise rotating vector. For a negative sequence, the corresponding one is a clockwise rotating vector. Zero sequence components will lead to a zero space vector.

Using the complex vector expression and transforming (8) into Laplace domain leads to

$$\begin{aligned} \vec{V}'_r(s) &= (r'_r + (s + j(\omega - \omega_m))L_{rr}) \vec{I}'_r(s) \\ &+ L_M (s + j(\omega - \omega_m)) \vec{I}_s(s) \end{aligned} \quad (11)$$

where $L_{ss} = L_{ls} + L_M$ and $L'_{rr} = L'_{lr} + L_M$. Hence, $I'_r(s)$ can be expressed by \vec{V}'_r and \vec{I}_s .

Converting (6) into Laplace domain and substituting the static current space vector according to (11) leads to

$$\begin{aligned} \vec{V}_s &= \left[r_s + (s + j\omega) \left(L_{ss} - \frac{L_M^2 [s + j(\omega - \omega_m)]}{r'_r + [s + j(\omega - \omega_m)]L_{rr}} \right) \right] \vec{I}_s \\ &+ \frac{(s + j\omega)L_M}{r'_r + [s + j(\omega - \omega_m)]L_{rr}} \vec{V}'_r. \end{aligned} \quad (12)$$

Therefore, a Thevenin equivalent circuit for the induction machine can be developed. Notice that the impedance $Z(s)$ is based on $DQ0$ reference frame. Since the RLC circuit is expressed in abc reference frame, it will be convenient that there is also an impedance model based on abc reference frame.

For three-phase systems, abc voltages and currents can be expressed as space vectors. The relation of a space vector and a static dq vector in time domain is known (10). In Laplace domain, their relation becomes

$$\vec{V}(s) = \vec{V}_{qds}(s - j\omega). \quad (13)$$

Hence, in space vector, the stator voltage can be expressed as follows by replacing s by $s - j\omega$ in (12):

$$\begin{aligned} \vec{V}(s) &= \left[r_s + (s - j\omega) \left(L_{ss} - \frac{L_M^2 [s - j\omega_m]}{r'_r + [s - j\omega_m]L_{rr}} \right) \right] \vec{I}_s \\ &+ \frac{sL_M}{r'_r + (s - j\omega_m)L_{rr}} \vec{V}'_r. \end{aligned} \quad (14)$$

If L_M is very large compared to the other parameters, then the above equation can be simplified as

$$Z_s(s) = r_s + s(L_{ls} + L'_{lr}) + \frac{s}{s - j\omega_m} r'_r. \quad (15)$$

The above derivation corroborates with the following analysis on slip. Slip is related to the rotating speed ω_m and the stator frequency ω . For the electric circuit analysis, the rotating speed can be assumed to be constant since mechanical dynamics is much slower than the electric dynamics. Slip can be expressed as $1 - \omega_m/\omega$. In Laplace domain, slip can be expressed as

$$\text{slip}(s) = \frac{s - j\omega_m}{s}. \quad (16)$$

Hence, the impedance of the DFIG seen from its terminal can be represented by

$$Z_{\text{DFIG}}(s) = r_r/\text{slip}(s) + r_s + (L_{ls} + L_{lr})s. \quad (17)$$

The above derivation also proves that the impedance model can be developed using the per-phase circuit of a DFIG. The simplified DFIG impedance in (17) ignoring RSC and GSC is adopted in [15].

C. Converter Impedance Model

Cascaded control loops are used in converters in wind generators. The control loops consist of the fast inner current control

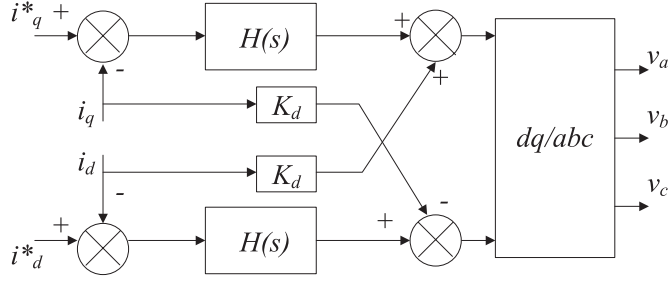


Fig. 4. Converter current control loops.

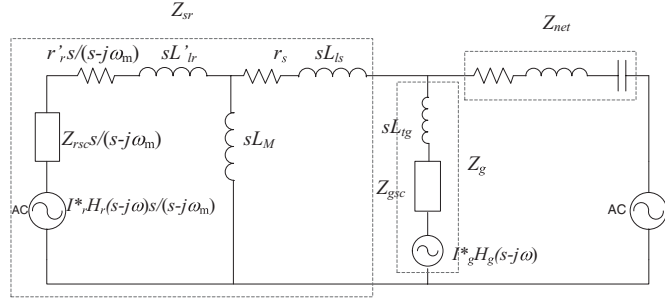


Fig. 5. Overall circuit model.

loops and the slow outer power/voltage control loops. The current control loops usually have bandwidths at or greater than 100 Hz, while the outer control loops usually have bandwidths less than several hertz. For SSR studies, the dynamics of interest are much faster than the outer control loops. Thus, the outer control is considered to be constant and will not be included in the impedance model.

For the vector current control scheme in Fig. 4, the qd -axis voltage and current relationship is

$$v_q = (i_q^* - i_q)H_i(s) - K_d i_d \quad (18)$$

$$v_d = (i_d^* - i_d)H_i(s) + K_d i_q. \quad (19)$$

This leads to the expression in complex vector:

$$\vec{V}_{qds} = \vec{I}_{qds}^* H(s) - (H(s) - jK_d) \vec{I}_{qds}. \quad (20)$$

To view the current-controlled converter from space vector

$$\vec{V} = \vec{I}^* H(s - j\omega) - (H(s - j\omega) - jK_d) \vec{I}. \quad (21)$$

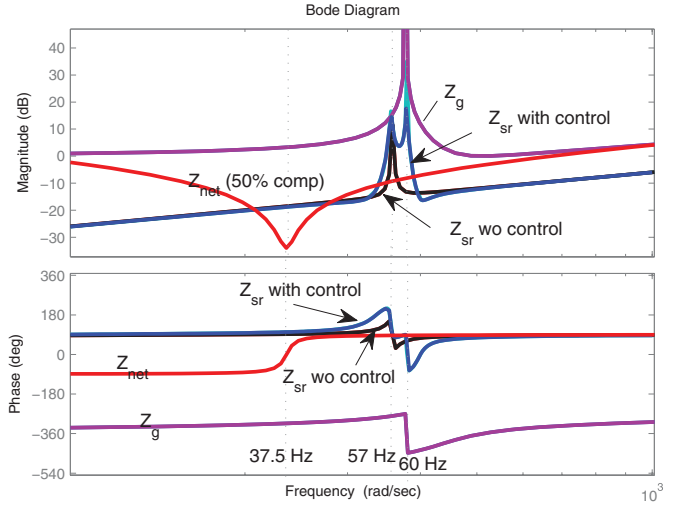
For the GSC at positive sequence scenarios, it can be represented by a voltage source $\vec{I}_g^* H_g(s - j\omega)$ behind an impedance Z_{gsc} , where $Z_{gsc} = H_g(s - j\omega) - jK_{dg}$.

For the RSC at positive sequence scenarios, it can also be represented by a voltage source $\vec{I}_r^* H_r(s - j\omega)$ behind an impedance Z_{rsc} , where $Z_{rsc} = H_r(s - j\omega) - jK_{dr}$.

D. Overall Circuit

The overall circuit is now shown in Fig. 5. The circuit consists of two impedance: the network impedance Z_{net} and the DFIG impedance Z_{DFIG} .

When the gains of the RSC controller K_p , K_i and the feed-forward gain K_{dr} are assumed to be zero, the RSC output voltage

Fig. 6. Bode plots of Z_g , Z_{net} , Z_{sr} .

will no longer vary even there exists error in measured currents and the reference currents. The RSC can be viewed as a constant voltage source in this case.

E. Comparison of Z_{sr} and Z_g

The DFIG impedance consists of two parallel components: the stator and rotor (including RSC) Z_{sr} and the GSC branch including the GSC and the filter: $Z_g = Z_{gsc} + sL_{tg}$. Bode plots of the RLC network impedances, Z_{sr} and Z_g at 95% rotating speed (or 57 Hz) and 50% compensation level, are plotted in Fig. 6. Z_{sr} is plotted for two scenarios: with and without current PI controllers. When the PI controller gain is not zero, Z_{sr} has two peaks: one at 57 Hz and the other at 60 Hz. When the gain is zero, Z_{sr} however has just one peak at 57 Hz. For Z_g , the resonant frequency is 60 Hz. The network impedance has a resonant frequency at 37.5 Hz, which correspond to the 50% compensation level. The network resonant frequency is expressed as

$$f_n = 60 \sqrt{\frac{X_c}{X_{line} + X_T}} \quad (22)$$

where X_c is the series capacitor reactance, X_{line} and X_T are the line reactance and the transformer reactance, respectively.

It is observed that at the interested SSR frequency region (< 37.5 Hz), the magnitude of Z_g is much larger than Z_{sr} . Therefore, Z_{sr} is dominant. For the following studies, the impact of Z_g will be ignored.

IV. NYQUIST-CRITERION-BASED STABILITY ANALYSIS

In this section, Nyquist-criterion-based stability analysis will be carried out to study the effect on SSR due to wind speed, compensation degree, and RSC PI controller gain. The expression of Z_{sr} can be found from the overall circuit shown in Fig. 5. The open-loop transfer function to be studied is Z_{net}/Z_{sr} and

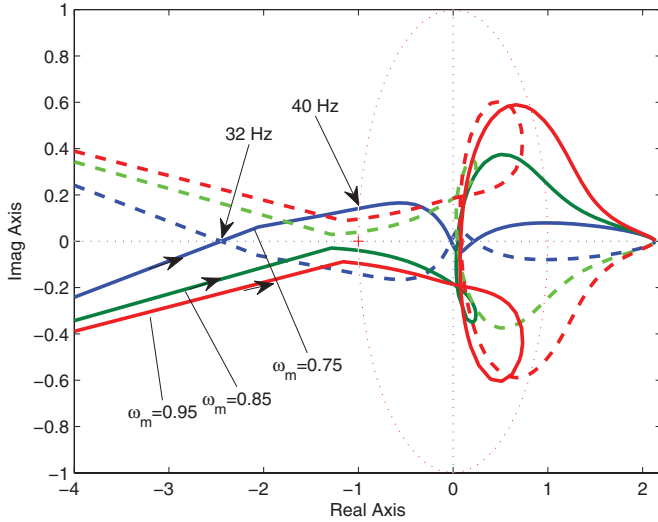


Fig. 7. Nyquist map for different rotating speeds. Series compensation level: 75%. Gains of the current controllers are zeros.

its expression is as follows:

$$\frac{Z_{net}}{Z_{sr}} = \frac{r + sL + \frac{1}{sC}}{r_s + sL_{ls} + \frac{sM(sL'_{lr} + \frac{s}{s-j\omega_m}(r'_r + K_p + \frac{K_i}{s-j\omega}) - jK_{dr})}{sM + sL'_{lr} + \frac{s}{s-j\omega_m}(r'_r + K_p + \frac{K_i}{s-j\omega}) - jK_{dr}}}. \quad (23)$$

A. Effect of Wind Speed

Using the same study system and same parameters as in [9], two impedances are derived and the Nyquist map of Z_{net}/Z_{sr} is plotted in Fig. 7. The gains of the RSC controllers are set to zeros. The compensation level is 75%. It is shown that when the rotating speed at 0.75 p.u., the Nyquist map will encircle $(-1, 0)$ which indicates instability. When the rotating speed is at 0.85 p.u. and 0.95 p.u., the Nyquist maps will not encircle $(-1, 0)$ and the system is marginally stable. The phase margins are 2° and 5° for the 0.85 p.u. and 0.95 p.u. rotating speed. The points when the Nyquist maps intersect with the unit circle have frequencies of about 40 Hz. This indicates the resonance frequency. It also corresponds to the LC resonant frequency at 75% compensation level.

The Nyquist map demonstrates the effect of wind speed on SSR stability since low wind speed corresponds to low rotating speed. Hence, a Type 3 wind generator is more prone to SSR when wind speed is lower.

B. Effect of Compensation Degree

The Bode plots of the network impedance Z_{net} at different compensation degrees and the DFIG impedance Z_{sr} are plotted in Fig. 8. The rotating speed is assumed to be 0.75 p.u. It is observed that a higher compensation degree results in a higher frequency at which $Z_{sr} = Z_{net}$: 251 rad/s (40 Hz) at 75% versus 206 rad/s (32.8 Hz) at 50%. It is also observed that the phase angle of Z_{sr} at that frequency is 107° at 75% compensation level compared to 95° at 50% compensation level. Therefore,

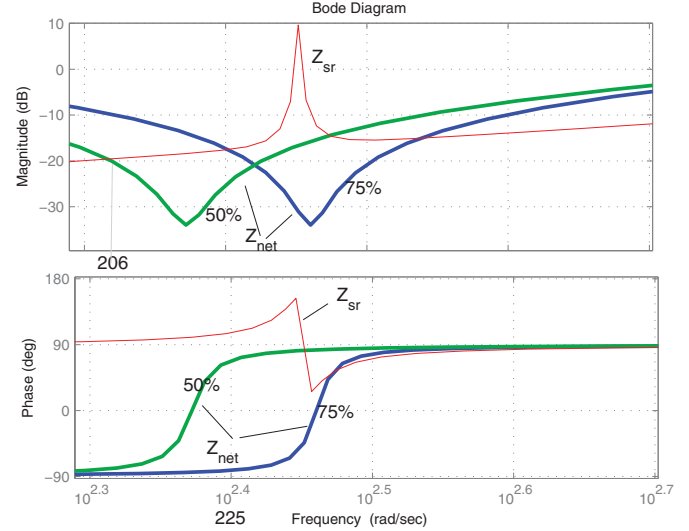


Fig. 8. Bode plots for Z_{net} at different compensation degree, Z_{sr} at Rotating speed 0.75 p.u.

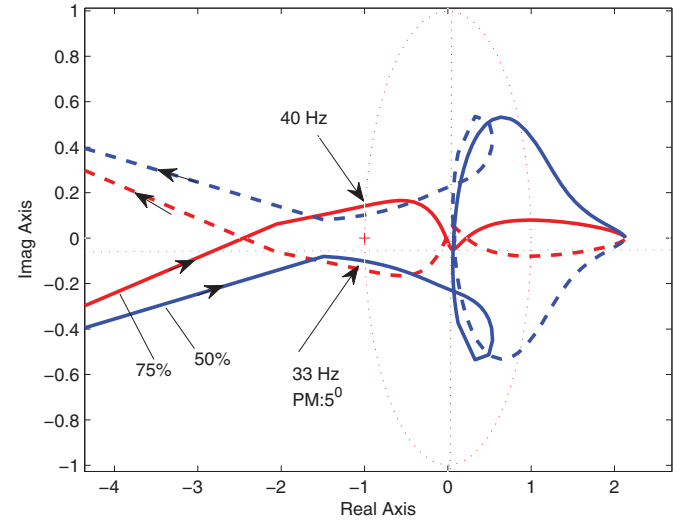


Fig. 9. Nyquist map for different compensation degree. Rotating speed: 0.75 p.u.

Z_{net}/Z_{sr} will have a less phase margin or become unstable when the compensation level is higher.

The Nyquist maps of the network Z_{net} and the DFIG impedance Z_{sr} at different compensation degrees are plotted in Fig. 9. The points where the Nyquist maps intersects the unit circle are at 33 Hz for 50% compensation level (phase margin 5°) and 40 Hz for 75% compensation level. The Nyquist maps indicate that $(-1, 0)$ is encircled at 75% compensation level. Hence, a higher compensation degree results in a less stable system.

C. Effect of RSC PI Controller Gain

In this section, the effect of the RSC PI controller gain is examined. The time constant of the PI controller is fixed at 0.02 s. The wind speed is selected as 9 m/s and the corresponding

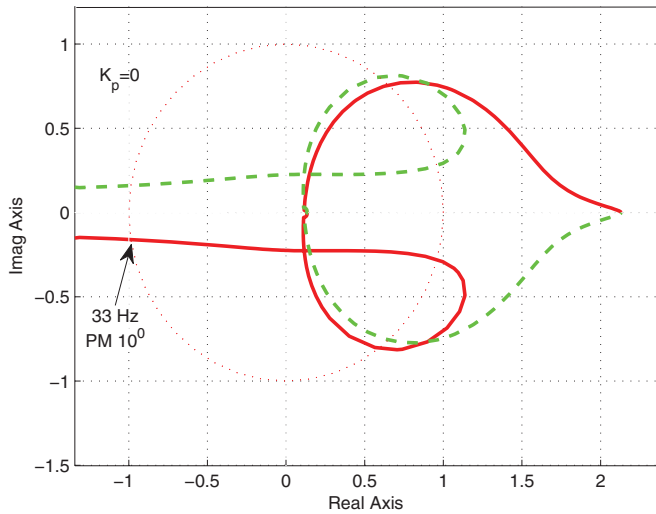


Fig. 10. Nyquist map when $K_p = 0$. Compensation level 50%. Rotating speed: 0.95 p.u.

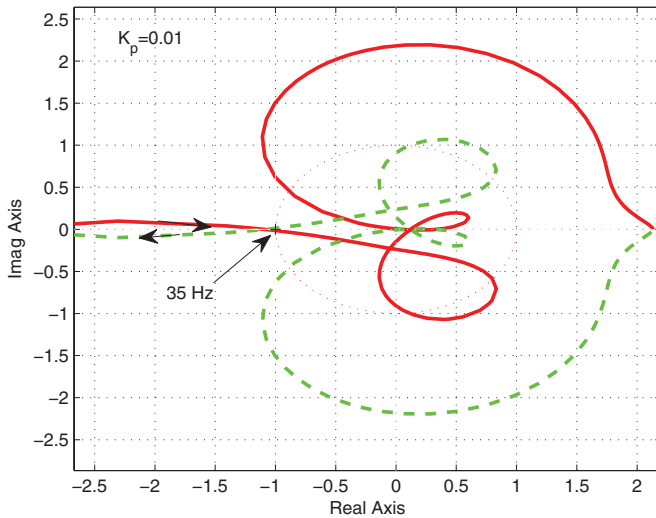


Fig. 11. Nyquist map when $K_p = 0.01$. Compensation level 50%. Rotating speed: 0.95 p.u.

rotating speed is 0.95 p.u. The compensation level is 50%. Two cases are examined.

- 1) Case 1: $K_p = 0$.
- 2) Case 2: $K_p = 0.01$.

The Nyquist plots are shown in Figs. 10 and 11. It is observed that when the gain is larger or equal to 0.01, the Nyquist maps encircle $(-1, 0)$ clockwise, which indicates instability. The point when the curve traverses the real axis is at 35 Hz. When the gain is zero, $(-1, 0)$ is not encircled and the phase margin is 11° at 33 Hz.

Bode plots of the impedances Z_{net} and Z_{sr} are shown in Fig. 12. It is shown that a higher current controller gain increases the magnitude of Z_{sr} and leads to a lower frequency at $Z_{net} = Z_{sr}$. The phase angle of the impedances at unit gain of Z_{net}/Z_{sr} are recorded in Table I.

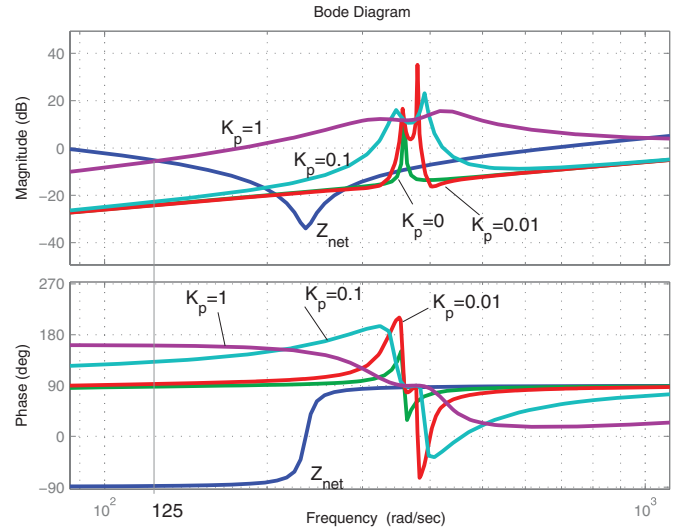


Fig. 12. Bode plots of Z_{sr} at different current controller gain.

TABLE I
PHASE ANGLES OF THE IMPEDANCES AND STABILITY DETECTION

	$K_p = 1$	$K_p = 0.1$	$K_p = 0.01$	$K_p = 0$
Res. Freq. (Hz)	20	32	35	33
$\angle Z_{net}$	-88°	-81.3°	-77°	-77°
$\angle Z_{sr}$	161°	149°	99.4°	91.4°
$\angle Z_{net}/Z_{sr}$	111°	130°	-178°	-168.4°
Stability	N	N	Marginal	stable

It is found that a higher gain leads to less phase margin or instability.

V. SIMULATION

The nonlinear model developed in [9] has been built in MATLAB/Simulink. The impact of wind speed and the RSC current loop control on SSR have also been discussed. It is observed that at lower wind speed, with high compensation level, the system is subject to SSR. The study in [9] focuses on low wind speed scenario. In this section, controller interaction between the RSC's current control and the electrical network will be verified. In [3], such phenomenon is classified as SSCI. The case study scenarios will be setup with wind speed at 9 m/s and the rotating speed at 95% of the nominal. The compensation level is 50%. The RSC control gain will be varied to show the impact of controller interaction.

- 1) Case 1: $K_p = 0.0$.
- 2) Case 2: $K_p = 0.01$.

The system is initially operated at 25% compensation level. At $t = 1$ s, additional capacitors are switched ON to make the compensation level reach 50%. Figs. 13–15 show the dynamic responses of the system with thick lines refer to Case 1, while the thin lines refer to Case 2. The dynamic responses of the electromagnetic torque, the rotating speed of the wind turbine, and the terminal voltage of the DFIG wind farm are shown Fig. 13. It is found that there is a resonance at about 25 Hz in the voltage magnitude and torque. For Case 1, the resonance can be damped out in the torque and the terminal voltage after 1 s.

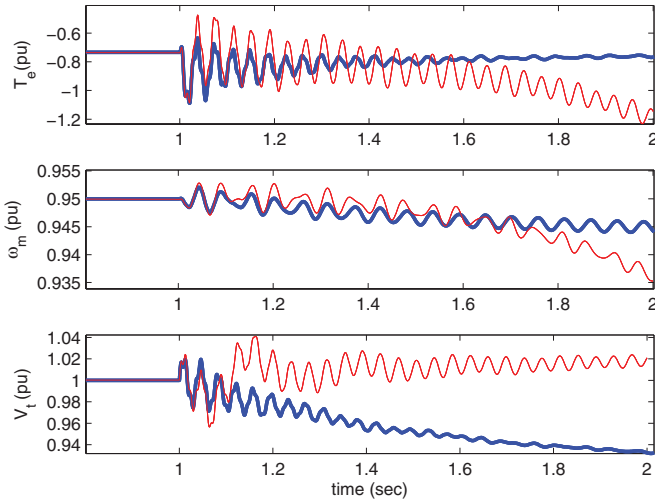


Fig. 13. Dynamic response of T_e , ω_m , and V_t . Thick lines: Case 1. Thin lines: Case 2.

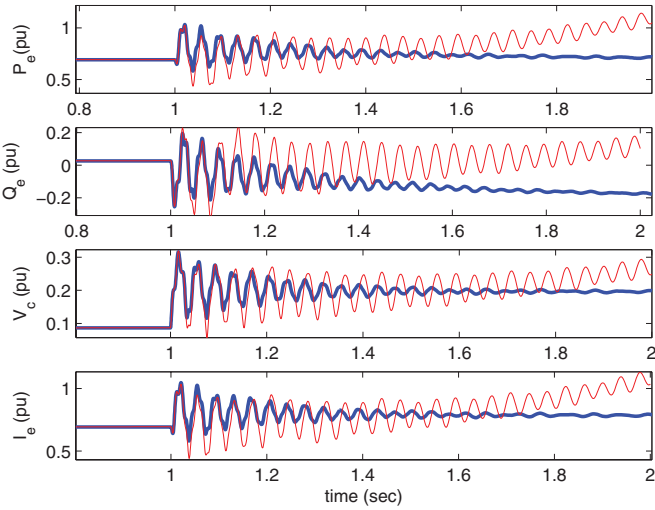


Fig. 14. Dynamic response of P_e , Q_e , V_c , and I_e . Thick lines: Case 1. Thin lines: Case 2.

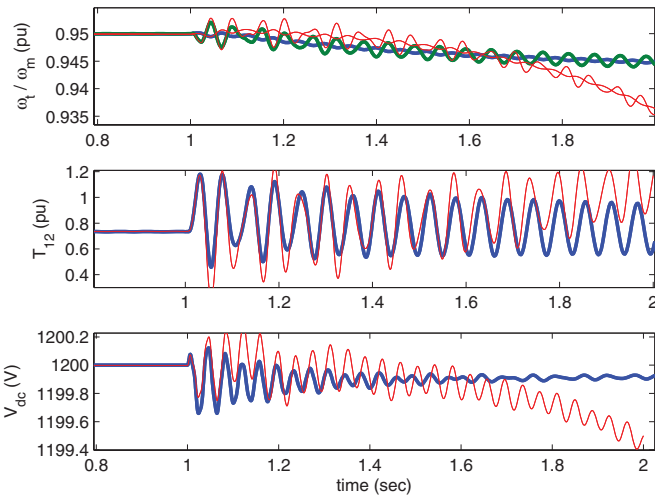


Fig. 15. Dynamic response of T_e , ω_m/ω_t , and V_{dc} . Thick lines: Case 1. Thin lines: Case 2.

However, for Case 2, the resonance cannot be damped out after 1 s.

Fig. 14 shows the dynamic responses of the DFIG wind farm output power P_e and Q_e , the voltage across the capacitors V_c , and the current through the line I_e . The resonance is damped out in Case 1 while persists in Case 2.

Fig. 15 shows the dynamic responses of the rotating speeds of two masses ω_t and ω_m , the torque T_{12} between the two masses of the wind turbine, and the dc-link voltage V_{dc} . The resonance is more obvious in Case 2. In addition, power/torque imbalance is observed that the rotating speed and the dc-link voltage keep decreasing.

According to the Nyquist/Bode analysis in Section III, the resonance is 35 Hz at 50% compensation level and 0.95 p.u. rotating speed. This resonance reflected in power, torque, and voltage/current magnitude will have a frequency of 25 Hz. The analysis in Fig. 11 also shows marginal stability or instability when the gain K_p is 0.01. Simulation results demonstrate the effect of current controller gain.

VI. CONCLUSION

This paper applies impedance-based Nyquist stability analysis to study Type 3 DFIG wind generator and series-compensated network SSR stability problems. Impedance models for a DFIG and a RLC network are first developed in space vector. Impacts of wind speed, compensation level, and RSC controller gain on SSR are examined applying Nyquist stability criterion. Both impedance-based Nyquist maps and Bode plots are used to demonstrate the impacts. Time-domain simulation results demonstrate the impact of current controller gain on SSR. The conclusion drawn based on impedance model and Nyquist stability criterion states that low wind speed is more problematic than high wind speed and RSC current control is detrimental to SSR stability.

APPENDIX

See Tables II–IV.

TABLE II
PARAMETERS OF A SINGLE 2-MW DFIG AND THE AGGREGATED DFIG IN THE NETWORK SYSTEM

Rated power	2 MW	100 MW
Rated voltage	690 V	690 V
X_{ls}	0.09231 pu	0.09231 pu
X_M	3.95279 pu	3.95279 pu
X_{lr}	0.09955 pu	0.09955 pu
R_s	0.00488 pu	0.00488 pu
R_r	0.00549 pu	0.00549 pu
H	3.5 s	3.5 s
X_{tg}	0.3 pu (0.189 mH)	0.3 pu ($\frac{0.189}{5}$ mH)
DC link capacitor C	14000 μF	50 \times 14000 μF
DC link rated voltage	1200 V	1200 V

TABLE III
PARAMETERS OF THE SHAFT SYSTEM

H_1	0.9 s
H_2	4.29 s
D_1	0 pu
D_2	0 pu
D_{12}	1.5 pu
K_{12}	50 pu

TABLE IV
PARAMETERS OF THE NETWORK SYSTEM

Transformer ratio	690V/161 kV
Base MVA	100 MVA
R_L	0.02 pu (5.1842 Ω)
X_L	0.5 pu (129.605 Ω)
X_C at 50% compensation level	64.8 Ω
Series compensation C	40 μ F
Line length	154 mile

REFERENCES

- [1] L. Gross, "Sub-synchronous grid conditions: New event, new problem, and new solutions," presented at the 37th Annu. Western Protect. Relay Conf., Spokane, WA, Oct. 2010.
- [2] (2011). Lesson learned: Sub-synchronous interaction between series-compensated transmission lines and generation. North American Electric Reliability Cooperation (NERC) [Online]. Available: http://www.nerc.com/files/LL_45_Sub-Synchronous_Interaction.pdf 2012.
- [3] G. Irwin, A. Jindal, and A. Isaacs, "Sub-synchronous control interactions between type 3 wind turbines and series compensated ac transmission systems," in *Proc. IEEE Power Energy General Meet.*, Jul. 2011, pp. 1–6.
- [4] (2010). Ercot crez reactive power compensation study. ABB [Online]. Available: http://www.uwig.org/CREZ_Reactive_Power_Compensation_Study.pdf
- [5] (2011). Lessons learned from interantional wind integration studies. Aemo Wind Integration WP4(A) [Online]. Available: <http://www.aemo.com.au/media/Files/Other/planning/0400-0051%20pdf.pdf>
- [6] G. Irwin, "Sub-synchronous interactions with wind turbines," presented at the Tech. Conf. CREZ System Design and Operation, EROT Taylor, TX, 2010.

- [7] A. Jindal, G. Irwin, and A. Woodord, "Sub-synchronous interactions with wind farms connected near series compensated ac lines," presented at the 9th International Workshop on Large-Scale Integration of Wind Power into Power Systems, Quebec City, QC, Canada, Oct. 2010.
- [8] C. Zhu, L. Fan, M. Hu, "Modeling and simulation of a DFIG-based wind turbine for SSR," presented at the North Amer. Power Symp., Mississippi State University, Mississippi State, MS, 2009.
- [9] L. Fan, R. Kavasseri, Z. Miao, and C. Zhu, "Modeling of DFIG-based wind farms for SSR analysis," *IEEE Trans. Power Del.*, vol. 25, no. 4, pp. 2073–2082, Oct. 2010.
- [10] A. Ostadi, A. Yazdani, and R. Varma, "Modeling and stability analysis of a DFIG-based wind-power generator interfaced with a series-compensated line," *IEEE Trans. Power Del.*, vol. 24, no. 3, pp. 1504–1514, Oct. 2009.
- [11] S. Atayde and A. Chandra, "Multiple machine representation of DFIG based grid-connected wind farms for SSR studies," in *Proc. 37th Annu. Conf. IEEE Ind. Electron. Soc.*, 2011, pp. 1468–1473.
- [12] J. Sun, "Small-signal methods for ac distributed power systems—A review," *IEEE Trans. Power Electron.*, vol. 24, no. 11, pp. 2545–2554, Nov. 2009.
- [13] J. Sun, "Impedance-based stability criterion for grid-connected inverters," *IEEE Trans. Power Electron.*, vol. 26, no. 11, pp. 3075–3078, Nov. 2011.
- [14] M. Cespedes and J. Sun, "Modeling and mitigation of harmonic resonance between wind turbines and the grid," in *Proc. IEEE Energy Convers. Congr. Expo.*, Sep. 2011, pp. 2109–2116.
- [15] L. Fan and Z. Miao, "Nyquist-stability-criterion based SSR explanation for type 3 wind generators," *IEEE Trans. Energy Convers.*, vol. 27, no. 3, pp. 807–809, Sep. 2012.
- [16] P. Krause, *Analysis of Electric Machinery*. New York: McGraw-Hill, 1986.



Zhixin Miao (S'00–M'03–SM'09) received the B.S.E.E. degree from the Huazhong University of Science and Technology, Wuhan, China, in 1992, the M.S.E.E. degree from the Graduate School, Nanjing Automation Research Institute, Nanjing, China, in 1997, and the Ph.D. degree in electrical engineering from West Virginia University, Morgantown, in 2002.

He is currently with the University of South Florida (USF), Tampa. Prior to joining USF in 2009, he was with the Transmission Asset Management Department with Midwest ISO, St. Paul, MN, from 2002

to 2009. His research interests include power system stability, microgrid, and renewable energy.